Peer-reviewed version available at Biomolecules 2018, 8, 13; doi:10.3390/biom8010013

Article

Amyloid Assembly Endows Gad m 1 with Biomineralization Properties

Milagros Castellanos [1], Rosa Rodriguez-Pérez[2] and María Gasset [3]

[1]IMDEA Nanoscience, Faraday 9, 28049 Madrid, Spain; milagros.castellanos@imdea.org
[2]Instituto de Investigación Hospital Universitario La Paz (IdiPaz), 28046 Madrid, Spain; rosa.rodriguez@idipaz.es
3Instituto Química-Física "Rocasolano", Consejo Superior de Investigaciones Científicas, 28006 Madrid, Spain; maria.gasset@csic.es

*Correspondence to: maria.gasset@csic.es; Tel.: +34-915619400

Abstract: Acid proteins capable of nucleating Ca^{2+} and displaying aggregation capacity play key roles in the formation of calcium carbonate biominerals. EF-hands are among the largest Ca^{2+}-binding motif in proteins. Gad m 1, an Atlantic cod β-parvalbumin isoform, is a monomeric EF-hand protein that acts as a Ca^{2+} buffer in fish muscle and is able to form amyloids under acidic conditions. Since nucleating Ca^{2+} protein have a propensity to form extended β-strand structures, we wondered whether amyloid assemblies of a protein containing refolded EF-hand motifs were able to influence the in vitro calcium carbonate crystallization. Here we have used the Gad m 1 chain as model to generate monomeric and amyloid assemblies and analyze their effect on in vitro calcite formation. We found that only amyloid assemblies alter calcite morphology.

Keywords: amyloids; Gad m 1, EF-hand motif, calcium carbonate precipitation, calcite

1. Introduction

Calcium carbonate biominerals are the most abundant natural biocomposites forming shells and balancing devices [**1,2**]. Acid proteins play major roles in the nucleation, growth and morphology of carbonate crystals by modulating Ca^{2+} condensation [**3-8**]. These proteins also share an oligomerization propensity involving extended β-strand structures, suggesting that amyloid protein assemblies with acidic regions could acquire biomineralization properties such as the modulation of calcium carbonate crystallization [**3, 9-11**].

Amyloid aggregates share the intermolecular cross-β sheet motif as scaffold and a variable morphology. These assemblies are usually unbranched fibrils with widths of 8–30 nm and lengths of μm that result from intertwisting of protofilaments made of pairs of β-sheets [**12,13**]. However, the shape and topology of the aggregate can be modified with changes in the sequence and in the conditions used for their formation [**14,15**]. Despite the variations in size and shape, all amyloids are featured by their structural repetitiveness and its interaction consequences [**12**]. For instance, Pmel amyloids allow the organized binding of melanin precursors and their efficient covalent polymerization into mature melanin [**16,17**]. In other cases, the amyloid fold of the segment dictates the apparition of novel binding sites absent in the monomer precursor such in the case of Zn^{2+} and the assembled Ac-IHVHLQI-$CONH_2$ peptide [**18,19**].

Among the distinct cation sites, the EF hand is a wide spread Ca^{2+}-binding motif. The EF hand is usually 30-residues long that folds into a helix-loop-helix structure in which the canonical 12-residues interhelical acid loop coordinates one cation with pentagonal bipyramidal symmetry [**9**]. This motif often occurs in pairs yielding the EF lobe [**20**]. Gad m 1, an Atlantic cod β-parvalbumin isoform with allergenic properties, represents a model of minimal EF-lobe protein [**21-23**]. Gad m 1 chain contains three tandemly arrayed EF-hands of which only the C-terminal two motifs named CD

and EF bind Ca^{2+}. As cation bound, Gad m 1 displays a highly stable monomeric helical globular fold [**24**]. On the contrary, removal of bound Ca^{2+} at high protein concentrations triggers Gad m 1 amyloid aggregation through the regions forming the helix B and D in the globular fold (Figure 1) [**25-27**]. Once formed, amyloids partially dissociate into monomers upon Ca^{2+} addition [**25**].

Here we have used the biocomposite-unrelated cod parvalbumin protein Gad m 1 amyloids to analyze their effect on calcium carbonate precipitation. We have found that amyloid assemblies but not monomers perturbed calcite crystallization from the conventional rhombohedral habit to a sheaf-like morphology.

2. Results

Figure 1 shows the sequence and structural features of Gad m 1 chain. The 109-residues chain is organized into three consecutive EF-hand motifs (AB, CD, EF) of which only CD and EF contain acid loops with functional Ca^{2+} binding. Of them, the regions B and D contain amyloid assembling sequences, defining alternation of amyloid-forming and Ca^{2+}-binding acid segments in the aggregated state [**26,27**]. Amyloid aggregation is regulated by the region sequence A which is C-terminal flanked by C19 as in all fish β-parvalbumins but lacks the N-terminal C12 featuring several isoforms [**25,26**]. This suggests that changing the Cys pattern may impact the amyloid state properties such as formation kinetics, morphology and stability [**28**]. Therefore, modification of Gad m 1 chain may allow the generation of distinct amyloids to evaluate the biomineralization activity.

With this in mind we generated Gad m 1 wt, I12C and C19S nd purified them in their Ca^{2+}-bound helical fold. The circular dichroism (CD) spectra, thermal denaturation curves and dynamic light scattering (DLS) analysis showed that I12C and C19S proteins display the characteristic monomeric α-helical fold of Gad m 1 wt (Figure 2A, 2B and 2C) [**25,26**].

To aggregate the chains in amyloids, protein solutions at 2 mg/ml were incubated in the presence of EDTA at 37 ^{o}C and the fluorescence changes of added thioflavin T (ThT) were followed with time. Figure 3A shows that on incubation all chains yielded a similar increase in the fluorescence intensity, but with differences in the lag-phases which inversely correlated with the number of Cys residues in the region A of the chain. Moreover, the increase in ThT fluorescence was accompanied by the formation of insoluble aggregates with β-sheet rich structure (Figure 3B) and anti-fibril OC antibody recognition by dot-blotting (Figure 3C), agreeing with the amyloid character of the aggregates.

Atomic force microscopy (AFM) analysis of the aggregates revealed that Gad m 1 wt forms mainly thin protofibrilar assemblies of 2.5 nm of height and lengths varying >300nm (Figure 4A), in agreement with previous work [**25**]. As with Gad m 1 wt, I12C aggregates appeared as short protofibrils of 3 nm of height but with a larger width (about 12 and 25 nm for wt and I12C protofibrils, respectively) (Figure 4B). On the contrary, Gad m 1 C19S aggregates displaying a distinct far-UV CD spectrum and similar content of OC-epitopes (Figure 3B), formed mainly rod-like nanoplatelets of 4 nm height, 50 nm width and 150 nm length (Figure 4C). Therefore amyloid aggregates formed with chains containing Cys residues flanking the segment A displayed protofibrilar morphologies, whereas Cys-free chains forms rod-like nanoplatelets. Thus, changing the disulfide bonding capacity by altering the Cys number allowed the generations of protofibrilar and platelet amyloid aggregates.

To determine the stability of the distinct polymers under the conditions required for calcium carbonate precipitation, aggregated proteins at 0.04 and 0.2 mg/ml final concentration were placed in 0.1 M $CaCl_2$ and the amount of protein in the soluble fraction of 100,000xg centrifugation determined. Under these conditions and as a function of protein concentration, aggregates partially dissociated yielding on average about 60 % of the protein as insoluble aggregate (Figure 3D). Despite the lack of significance among the differences, the data suggested the protofibrillar amyloids formed by chains containing Cys residues (wt and I12C) resisted better the solubilizing action of Ca^{2+} than the nanoplatelets formed by the C19S chain.

Preprints (www.preprints.org) | NOT PEER-REVIEWED | Posted: 18 January 2018 doi:10.20944/preprints201801.0172.v1

Peer-reviewed version available at Biomolecules 2018, 8, 13; doi:10.3390/biom8010013

To investigate the influence of amyloids on calcium carbonate precipitation, aggregates were placed under the previous conditions and the reaction was allowed by controlled diffusion of CO_2 from the decomposition of ammonium carbonate. As control for non-polymerized and Ca^{2+} pre-complexed protein form we used Ca^{2+}-bound Gad m 1 wt monomers at similar concentrations [**24**,**25**]. The representative crystal structures formed were visualized by scanning electron microscopy (SEM) (Figure 5). In the absence of protein the common rhombohedral habit of calcite crystals was observed (Figure 5A). Reactions performed in the presence of Gad m 1 monomers yielded rhombohedral calcite crystals with smooth surfaces (Figure 5B). These data indicated that the globular fold of Gad m 1 had a weak influence on calcite morphology. In other words, the acid loops of the folded EF-lobe do not participate in the crystallization process. On the contrary, presence of Gad m 1 wt, I12C and C19S amyloids caused the precipitation in distinct cylindrical and sheaf-like crystals (Figure 5C, 5D and 5E). These changes were proportional to the protein concentration used. Importantly, despite shape similarities each of the aggregates caused specific morphological signatures. In this sense, Gad m1 wt protofibrils yielded 75 μm long cylindrical and sheaf-like crystals with 45-50 μm diameters with capping regular surfaces (Figure 5C). The crystals obtained in the presence of I12C protofibrils were mostly sheaf-like morphologies of 125 μm lengths and 70 μm diameters, with regular capping surfaces (Figure 5D). Nanoplatelets of C19S mutant yielded smaller crystals consisting in a mixture of cylinders (25 and 50 μm length and diameter, respectively) and tightly tide sheaf (Figure 5E). Therefore these data show that the geometry of the acid loops in the amyloid aggregates promote the formation of nucleation centers that directly influence calcite crystallization.

2.2. Figures.

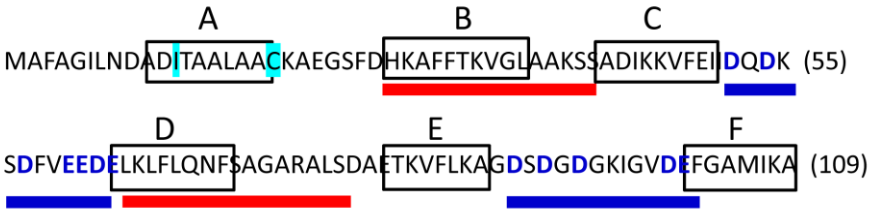

Figure 1. Gad m 1 chain and structural features. Gad m 1 sequences codes two folds. In the globular fold, segments AB, CD and EF adopt a helix-loop-helix structure of EF-hands maintained by Ca^{2+} binding to the acid loops (blue thick lines) joining C and D, and E and F helices (rectangles). The amyloid fold is maintained by the assembly of the segments underlined in red and the released of bound cations. Positions for the generation of the point mutants I12C and C19S affecting amyloid assembly are shadowed in cyan.

Preprints (www.preprints.org) | NOT PEER-REVIEWED | Posted: 18 January 2018 doi:10.20944/preprints201801.0172.v1

Peer-reviewed version available at Biomolecules 2018, 8, 13; doi:10.3390/biom8010013

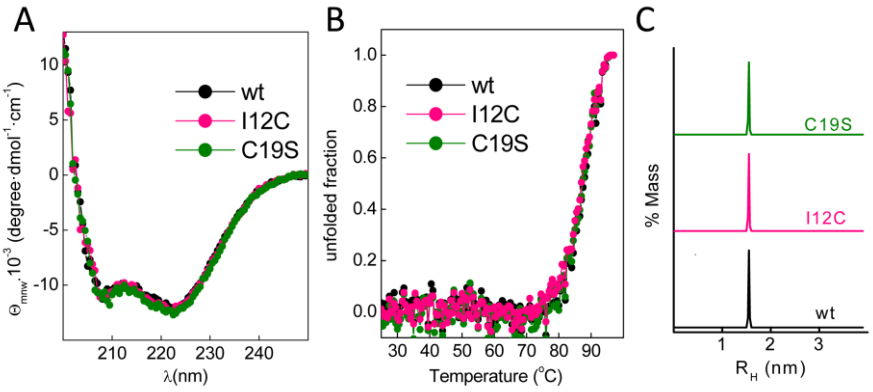

Figure 2. Conformational features of the Ca2+-bound fold of Gad m 1 wt and mutant. (A) Far-UV CD spectra of Ca^{2+}-bound Gad m 1 chains depicting their helical fold. **(B)** Thermal denaturation of Ca^{2+}-bound Gad m 1 chains displaying the cooperativity and stability of their folds. Denaturation curves were obtained from the changes in the molar ellipticity at 222 nm upon heating. **(C)** DLS analysis of Ca^{2+}-bound Gad m 1 chains shows Rh values compatible with monomeric states.

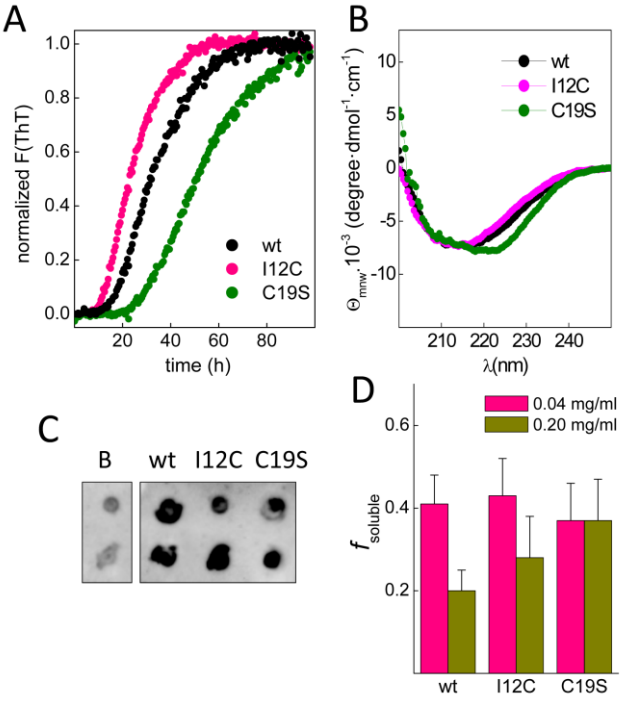

Figure 3. Amyloid aggregation of Gad m 1 chains. (A) Kinetics of amyloid aggregation followed by ThT fluorescence. **(B)** CD spectra of Gad m 1 aggregates isolated by ultracentrifugation. (C) Dot-blot analysis of the recognition of the aggregation reaction products by the anti-amyloid OC fibrils antibody (OC). The background (B) was obtained with the aggregation buffer. **(D)** Amyloid dissociation in 0.1 M $CaCl_2$ measured as the molar fraction of protein detected in the soluble phase ($f_{soluble}$) of a 100,000xg ultracentrifugation**.**

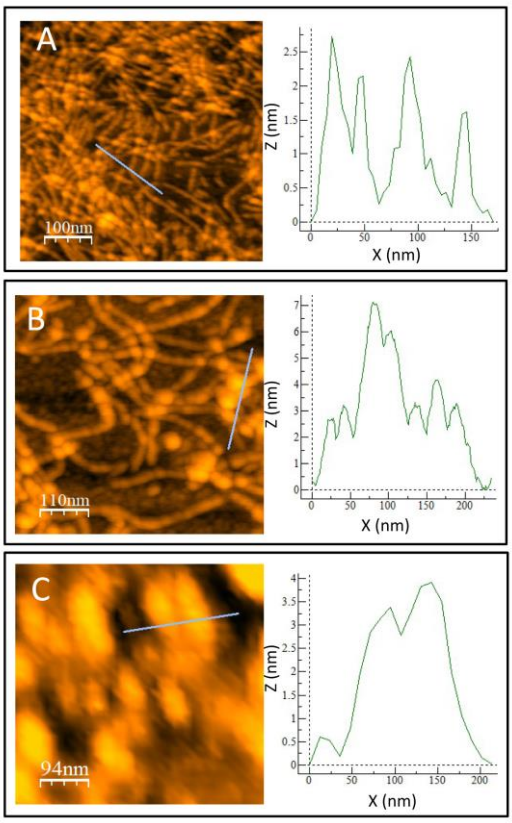

Figure 4. Atomic force micrographs of Gad m 1 amyloid assemblies. Images of the aggregation products of Gad m 1 (**A**) wt, (**B**) I12C and (**C**) C19S with the height profiles corresponding to the displayed bars.

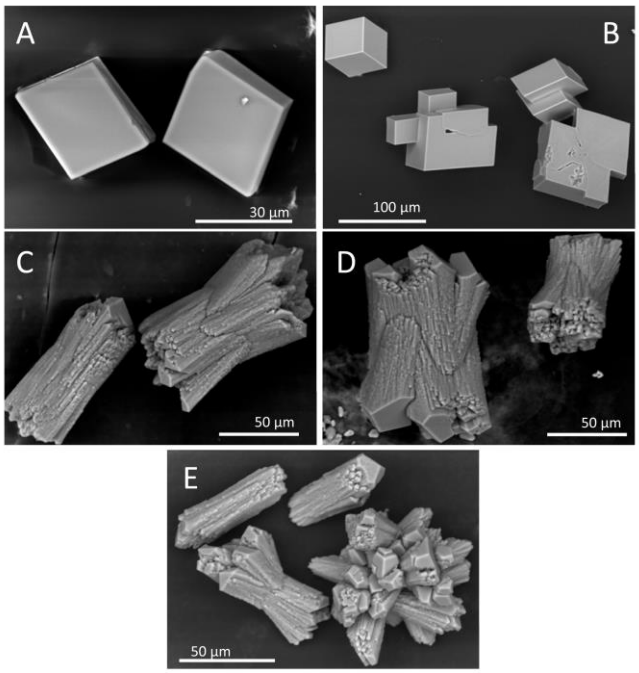

Figure 5. SEM images of in vitro calcite crystallization. $CaCO_3$ crystals were obtained in the (**A**) absence and presence of Gad m 1 (**B**) wt monomer, (**C**) wt amyloids, (**D**) I12C amyloids and (**E**) C19S amyloids. Protein concentration was 0.2 mg/ml.

3. Discussion

Current research has shown that amyloid aggregates constitute a basic scaffold for their functional exploitation in material science such as the generation biominerals. In the present study we asked whether amyloid assemblies of a protein with acid regions can acquire biomineralization properties such as a calcium carbonate crystallization modulation. To test this hypothesis we have used Gad m 1. This fish β-parvalbumin can transition from a three EF-hand globular fold to a β-sheet rich amyloid aggregate by changing the Ca^{2+} binding to the C-terminal acid loops. Gad m 1 amyloids are supported by the assembly of the regions B and D whereas the acid loops join regions CD and EF (Figure 1). This design differs from that of the self-assembling β-peptide P11-4 (Ace-QQRFEWEFEQQ-NH2) use for other Ca^{2+} nucleating reactions [**29**]. Our study revealed that Gad m 1 amyloids formed with distinct chains influences calcium carbonate crystallization, causing the appearance of different cylindrical and sheaf-like morphologies, contrasting the characteristic rhombohedral habit of calcite. Importantly, each amyloid assembly imprinted specific characteristics to the crystals.

Apart from the well-known Ca^{2+}-buffering physiological role of Gad m 1 globular fold, recently the ability to form the amyloid aggregates has been associated to an augmented IgE recognition in food allergies [**21-25**]. Notwithstanding, the capacity of these amyloids to modulate calcium carbonate precipitation makes them environmentally friendly tools, such as in protection of decayed stones or in CO_2 deposition devices. It must be mentioned that Gad m 1 amyloids mainly trap CO_2 using bound Ca^{2+}, whereas other amyloid-based traps uniquely bind the CO_2 by carbamate formation with their Lys residues [**30**]. Functioning of these alternate mechanisms support designs of hybrid amyloids (with the optimal Lys content at the core and the appropriate flanking acid segment) for the amplification of $C0_2$ deposition efficiency.

Calcite crystallizes in layers and differences in the relative growth rates in the distinct axes impacts the shape and morphology of crystals [**31,32**]. The use of assemblies formed with Gad m 1 mutants differing in the Cys content showed a common pattern of modification in the relative growth rates yielding morphologies distinct from those generated by biocomposite related and unrelated proteins [**2-11,31-34**]. However crystals displayed chain-dependent features supporting the imprint of amyloid differences. For instance, the size of the obtained crystals was higher in the reactions using protofibrils (produced by Gad m 1 wt and I12C mutant) than in those using nanoplatelet-like assemblies formed by Gad m 1 C19S. On the other hand, the two protofibrilar assemblies used also yielded differences in the diameter of the cylindrical crystals which correlate with the assembly widths. Importantly, Gad m 1 monomers in which the acid loops define the Ca^{2+} binding site have a weak influence in calcite crystallization. It must be noted, that the absence of major effects with the monomer underscored the role of surface charges such as those reported for the aggregates formed by the egg-shell forming ovocleidin-17 [**33**].

Calcium carbonate particles are appealing due to applications in the removal of heavy metal ions from waters, improvement of mechanical properties of foam, and in the generation of ultrasonic-sensitive drug delivery devices [35]. Despite much work is needed, our results provide a proof of concept for the functional exploitation of a non-physiological amyloid in the field of calcium carbonate-based material.

4. Materials and Methods

4.1. Production of Gad m1 wt and mutant chains. Gad m 1 (UniProtKB A5I874) was produced from a pET15b construct previously described [**25**]. Mutants I12C and C19S were generated using Quickchange protocols and the oligos (only forward) 5′-CGATGCGGATTGCACCGCGGCG-3′ and 5′-GCGCTGGCGGCGAGCAAAGCGGAAGGC-3′. Changes were verified by sequencing. All

proteins were produced in E.coli BLD21 (DE3), isolated and purified as described [**26**]. The N-terminal His-tags were removed using Thrombin CleanCleave™ kit following the manufacturer indications (Sigma). Before their use, protein solutions were extensively dialyzed against 5 mM Hepes pH 7.5 containing 0.1 mM $CaCl_2$, concentrated using 10 kDa-pore size Amicon Ultra-15 and centrifuged at 16,000×g for 20 min at 4 ºC to remove aggregates. Protein concentrations were determined using Bradford protein assay (Biorad) [**26**].

4.2. Circular dichroism spectroscopy. Circular dichroism measurements were performed using a Jasco J-820 spectropolarimeter using 0.1-cm cuvettes and thermostated cell holder. Spectra were recorded using 20 μM protein solutions in 10 mM Tris-HCl pH 7.5 containing 35 mM NaCl and 5 mM $CaCl_2$. For thermal denaturation experiments, Tris-HCl was replaced by Hepes-HCl and the ellipticity changes at 222 nm upon heating from 15 °C to 90 °C at a 1 degree/min heating rate were monitored. Both, spectra and denaturation curves were analyzed as described [**25,26**].

4.3. Dynamic Light Scattering. Dynamic light scattering (DLS) analyses were performed in a DynaPro spectroscatter (Wyatt Technology) at 25 °C using a thermostated 30 μL quartz cuvette. The hydrodynamic radii (R_H) and mass proportions (%) of the species were derived from the average of 20 acquisitions using cumulative fit as described [**25**]. Measurements were performed in duplicates using two different protein batches.

4.4. Amyloid formation and stability. Amyloid aggregates were formed by incubating proteins (2 mg/ml) in 25 mM Tris-HCl pH 7.5 containing 50mM NaCl and 4 mM EDTA for 120 h at 37 ºC. Briefly, protein stocks cleared from aggregates by centrifugation were diluted with 25 mM Tris-HCl pH 7.5 containing 50 mM NaCl, 4 mM EDTA and supplemented or not with 10 μM ThT (Calbiochem) for fluorescence reading experiments. Reactions were initiated by placing the sealed 96-well plate (0.150 ml of solution/well) at 37 °C in a POLARstar (BMG Labtech) microplate reader. The ThT fluorescence was measured through the bottom of the plate every 30 min with a 450 nm excitation filter and a 480 nm emission filter in the absence of agitation. All measurements were performed in triplicates, and the experiment was repeated using at least two different protein batches. When required, aggregates were harvested from the reaction mixtures performed in the absence of ThT by a 100.000xg centrifugation for 1 h using an Optima TM^{Max} Beckman ultracentrifuge. The obtained pellets were resuspended at 2 mg/ml in 25 mM Tris-HCl pH 7.5, 50 mM NaCl and stored at room temperature until use**.** Aggregates from Gad m 1 chains were diluted in 0.1M $CaCl_2$ at 0.04 and 0.2mg/ml. After 1 h of incubation, samples were centrifuged for 1 h at 100,000xg using an Optima TM^{Max} Beckman ultracentrifuge and the protein content in both soluble and pellet fractions determined using the Bradford protein assay.

4.5. Dot-blot analysis. Aliquots containing 100 ng of Ca^{2+}-bound monomers and amyloids of Gad m 1 chains were spotted in duplicates on a nitrocellulose membrane. Immunodetection was performed by 1 h incubation with the anti-amyloid fibrils OC antibody (AB2286 Merck Millipore, 1/2000 dilution), followed by extensive washes and 30 min incubation with horseradish peroxidase-labeled goat anti-rabbit IgG (1:5000 diluted; Sigma) [25,26]. The ECL-Western-blotting reagent (Biorad) and a ChemiDoc XRS equipment (BioRad) were used for signal development and detection, respectively.

4.6. Atomic Force Microscopy. For AFM visualization, the products of the aggregation reactions were diluted 1/10 in 25 mM Tris-HCl pH 7.5, 50 mM NaCl, 4 mM EDTA. Typically, 30 μl of the resulting solutions were absorbed onto freshly cleaved mica by 5-10 min incubations at room temperature. Surfaces were then rinsed with double distilled water and dried. Images were obtained using a MultiMode Veeco microscope with a NanoScope IIIa controller using rectangular cantilevers with tetrahedral tips (Oltespa, 2N/m force constant and 70 KHz resonance frequency). Software to obtain and treat the images where supplied with the instrumentation (NanoScope). AFM analysis was performed using the WSxM 4.0 free software (Nanotec).

4.7. Crystal Growth Experiments. Crystallization experiments were performed at 18 °C using sterile Lab-Tek chambers with slides with covers inside a desiccator for $CaCO_3$ crystal synthesis. Chambers in permanox porta were supplement with 50-µl of 0.1 M $CaCl_2$. For each experiment performed in duplicate, 1 and 5 µl of protein solutions (2 mg/ml) were added to the droplet. Chambers were sealed with parafilm, then pierced with a needle, and placed in a desiccator. The constant CO_2 vapor pressure for diffusion was generated by the decomposition of ammonium carbonate (25 mM) contained in 5 ml beakers. After 20 h the crystals were rinsed first with Milli-Q water and then with $CaCl_2$-saturated methanol and allowed to air-dry. Analysis was performed using a Hitachi S-3000N scanning electron microscopy at 20 kV in the Scanning Microscopy Unit of the University Autónoma of Madrid.

Acknowledgments: This work was supported by grants from Spanish AEI/EU-FEDER SAF2014-52661-C3 and BFU2015-72271-EXP. Raquel Pérez-Tavares is acknowledged for her excellent technical support. Antonio Romero is acknowledged for his indications for the crystallization set-up.

Author Contributions: MG conceived and designed the experiments; MC, RRP and MG performed the experiments and analyzed the data; MC, RRP and MG wrote the paper.

Conflicts of Interest: The authors declare no conflict of interest

References

1. Mann, S. Biomineralization: principles and concepts in bioinorganic materials chemistry. New York: Oxford University Press, **2001**.
2. Feng, Q. (2011) Principles of Calcium-Based Biomineralization. Molecular Biomineralization. Progress in Molecular and Subcellular Biology **2011**, 52, 141-197.
3. Evans, JS. "Tuning in" to mollusk shell nacre- and prismatic-associated protein terminal sequences. Implications for biomineralization and the construction of high performance inorganic-organic composites. *Chem Rev.* **2008**, 108,4455-4462.
4. Takeuchi, T.; Sarashina, I.; Iijima, M.; Endo, K. In vitro regulation of CaCO(3) crystal polymorphism by the highly acidic molluscan shell protein Aspein. *FEBS Lett.* **2008**, 582, 591-596.
5. Fang, D.; Pan, C.; Lin, H.; Lin, Y.; Zhang, G.; Wang, H.; He, M.; Xie, L.; Zhang, R. Novel basic protein, PfN23, functions as key macromolecule during nacre formation. .*J. Biol. Chem.* **2012**, 287, 15776-15785.
6. Isowa, Y.;, Sarashina, I.; Setiamarga, D.H.; Endo, K. A comparative study of the shell matrix protein aspein in pterioid bivalves. *J. Mol. Evol.* **2012**, 75,11-18.
7. Perovic, I.; Mandal, T.; Evans, J.S. A pearl protein self-assembles to form protein complexes that amplify mineralization. *Biochemistry* **2013**, 52, 5696-5703.
8. Chang, E.P.; Evans, J.S. Pif97, a von Willebrand and peritrophin biomineralization protein, organizes mineral nanoparticles and creates intracrystalline nanochambers. *Biochemistry* **2015**, 54, 5348-5355.
9. Persechini, A.; Moncrief, N.D.; Kretsinger, R.H. The EF-hand family of calcium-modulated proteins. *Trends Neurosci.* **1989**,12, 462-467.
10. Perovic, I.; Chang, E.P.; Lui, M.; Rao, A.; Cölfen, H.; Evans, J.S. A nacre protein, n16.3, self-assembles to form protein oligomers that dimensionally limit and organize mineral deposits. *Biochemistry* **2014**, 53, 2739-2748.
11. Jain, G.; Pendola, M.; Huang, Y.C.; Colas, J.; Gebauer, D.; Johnson, S.; Evans, J.S. Functional prioritization and hydrogel regulation phenomena created by a combinatorial pearl-associated two-protein biomineralization model system. *Biochemistry* **2017**, 56, 3607-3618.
12. Riek, R.; Eisenberg, D.S. The activities of amyloids from a structural perspective. *Nature* **2016**, 539, 227-235.
13. Eisenberg, D.S.; Sawaya, M.R. Structural Studies of Amyloid Proteins at the Molecular Level. *Annu. Rev Biochem.* **2017**, 86, 69-95.
14. Knowles, T.P.; Mezzenga, R. Amyloid Fibrils as Building Blocks for Natural and Artificial Functional Materials. *Adv. Mater.* **2016**, 28, 6546-6561.
15. Wei, G.; Su, Z.; Reynolds, N.P.; Arosio, P.; Hamley ,I.W.; Gazit, E.; Mezzenga, R. Self-assembling peptide and protein amyloids: from structure to tailored function in nanotechnology. *Chem Soc Rev.* **2017**, 46, 4661-4708.

16. McGlinchey, R.P.; Shewmaker, F.; McPhie, P.; Monterroso, B.; Thurber, K.; Wickner, R.B. The repeat domain of the melanosome fibril protein Pmel17 forms the amyloid core promoting melanin synthesis. *Proc. Natl. Acad. Sci. U S A*. **2009**, 106, 13731-13736.
17. Bissig, C.; Rochin, L.; van Niel, G. PMEL amyloid fibril formation: the bright steps of pigmentation. *Int J Mol Sci.* **2016**, 17, E1438.
18. Bolisetty, S.; Mezzenga, R. Amyloid-carbon hybrid membranes for universal water purification. *Nat Nanotechnol*. **2016**, 11, 365-371.
19. Lee, M.; Wang, T.; Makhlynets, O.V.; Wu, Y.; Polizzi, N.F.; Wu, H.; Gosavi, P.M.; Stöhr, J.; Korendovych, I.V.; DeGrado, W.F.; Hong, M. Zinc-binding structure of a catalytic amyloid from solid-state NMR. *Proc Natl Acad Sci U S A.* **2017**, 114, 6191-6196.
20. Kawasaki, H.; Kretsinger, R.H. Structural and functional diversity of **EF**-hand proteins: Evolutionary perspectives. *Protein Sci.* **2017**, 26, 1898-1920.
21. Kuehn, A.; Swoboda, I.; Arumugam, K.; Hilger, C.; Hentges, F. Fish allergens at a glance: variable allergenicity of parvalbumins, the major fish allergens. *Front Immunol.* **2014**, 5:179.
22. Sharp, M.F.; Lopata, A.L. Fish allergy: in review. *Clin Rev Allergy Immunol.* **2014**, 46,258-271.
23. Permyakov, E.A.; Uversky, V.N.; Permyakov, S.E. Parvalbumin as a Pleomorphic Protein. *Curr Protein Pept Sci.* **2017**, 18, 780-794.
24. Moraes, A.H.; Ackerbauer, D.; Kostadinova, M.; Bublin, M.; de Oliveira, G.A.; Ferreira, F.; Almeida, F.C.; Breiteneder, H.; Valente, A.P. Solution and high-pressure NMR studies of the structure, dynamics, and stability of the cross-reactive allergenic cod parvalbumin Gad m 1. *Proteins* **2014** 82, 3032-3042.
25. Martínez, J.; Sánchez, R.; Castellanos, M.; Fernández-Escamilla, A.M.; Vázquez-Cortés, S.; Fernández-Rivas, M.; Gasset, M. Fish β-parvalbumin acquires allergenic properties by amyloid assembly.*Swiss Med Wkly* **2015**, 145:w14128.
26. Sánchez, R.; Martínez, J.; Castro, A.; Pedrosa, M.; Quirce, S.; Rodríguez-Pérez, R.; Gasset, M. The amyloid fold of Gad m 1 epitopes governs IgE binding. *Sci Rep*. **2016,** 6, 32801.
27. Sánchez, R.; Martínez, J.; Montoya, L.; Castellanos, M.; Gasset, M. Mapping Amyloid Regions in Gad m 1 with Peptide Arrays. *Methods Mol Biol*. **2018**, in press
28. Martínez, J.; Sánchez, R.; Castellanos, M.; Makarava, N.; Aguzzi, A.; Baskakov, I.V.; Gasset, M. PrP charge structure encodes interdomain interactions. *Sci Rep*. **2015**, 5, 13623.
29. Brunton,P.A.; Davies, R.P.; Burke, J.L.; Smith, A.; Aggeli, A.; Brookes, S.J.; Kirkham, J. Treatment of early caries lesions using biomimetic self-assembling peptides--a clinical safety trial. *Br Dent J.* **2013** 215, E6.
30. Li, D.; Jones, E.M.; Sawaya, M.R; Furukawa, H.; Luo, F.; Ivanova, M.; Sievers, S.A.; Wang, W.; Yaghi, O.M.; Liu, C.; Eisenberg, D.S. Structure-based design of functional amyloid materials. *J Am Chem Soc*. **2014**, 136, 18044-18051.
31. Wang, R.Z.; Addadi, L.; Weiner, S. Design strategies of sea urchin teeth: structure, composition and micromechanical relations to function. *Philos Trans R Soc Lond B Biol Sci* **1997**, 352, 469–480.
32. Weiner, S.; Addadi, L. Acidic macromolecules of mineralized tissues: the controllers of crystal formation. *Trends Biochem Sci* **1991**, 16, 252–256.
33. Reyes-Grajeda, J.P; Moreno, A.; Romero, A. Crystal structure of ovocleidin-17, a major protein of the calcified Gallus gallus eggshell: implications in the calcite mineral growth pattern. *J Biol Chem*. **2004**, 279, 40876-40881.
34. Polowczyk, I.; Bastrzyk, A.; Fiedot, M. Protein-mediated precipitation of calcium carbonate. *Materials (Basel)*. **2016**, 9, E944.
35. Declet, A.; Reyes, E.; Suarez, O.M. Calcium carbonate precipitation: a review of the carbonate crystallization process and applications in bioinspired composites. *Rev. Adv. Mater. Sci.* **2016**, 44, 87-107.